1 **A biosensor to gauge protein homeostasis resilience differences in the nucleus compared to**

2 **cytosol of mammalian cells**

3 Candice B. Raeburn[1], Angelique Ormsby[1], Nagaraj S. Moily[1], Dezerae Cox[1], Simon Ebbinghaus[2], Alex

4 Dickson[3], Gawain McColl[4] and Danny M. Hatters[1,*]

5 [1]Department of Biochemistry and Pharmacology; and Bio21 Molecular Science and Biotechnology

6 Institute, The University of Melbourne, VIC 3010. Australia

7 [2]Physical and Theoretical Chemistry, TU Braunschweig, 38106 Germany and Braunschweig

8 Integrated Centre of Systems Biology, 38106 Germany

9 [3]Department of Biochemistry & Molecular Biology, Michigan State University, East Lansing, MI,

10 48824, USA

11 [4]Melbourne Dementia Research Centre, Florey Institute of Neuroscience and Mental Health and

12 University of Melbourne, Parkville, VIC 3052, Australia.

13 *Correspondence:* dhatters@unimelb.edu (D.M. Hatters).

14

15 **Abstract**

16 An extensive network of chaperones and other proteins maintain protein homeostasis and guard

17 against inappropriate protein aggregation that is a hallmark of neurodegenerative diseases. Using a

18 fluorescence resonance energy-based biosensor that simultaneously reports on intact cellular

19 chaperone holdase activity and detrimental aggregation propensity, we investigated the buffering

20 capacity of the systems managing protein homeostasis in the nucleus of the human cell line HEK293

21 compared to the cytosol. We found that the nucleus showed lower net holdase activity and reduced

22 capacity to suppress protein aggregation, suggesting that the nuclear quality control resources are

23 less effective compared to those in the cytosol. Aggregation of mutant huntingtin exon 1 protein

24 (Httex1) in the cytosol appeared to deplete cytosolic chaperone supply by depleting holdase activity.

25 Unexpectedly, the same stress increased holdase activity in the nucleus suggesting that proteostasis

26 stress can trigger a rebalance of chaperone supply in different subcellular compartments.

27 Collectively the findings suggest the cytosol has more capacity to manage imbalances in proteome

28 foldedness than the nucleus, but chaperone supply can be redirected into the nucleus under

29 conditions of proteostasis stress caused by cytosolic protein aggregation.

30

Introduction

Protein homeostasis involves a network of quality control systems that ensures the proteome is properly translated, folded, delivered to the correct cellular location and turned over at appropriate times. When protein homeostasis becomes unbalanced, proteins become prone to misfolding leading to their mislocalisation and accumulation as aggregates (1,2). The imbalance of protein homeostasis is hypothesized to underlie the inappropriate protein misfolding and aggregation that arise in the brain of patients with common neurodegenerative diseases including Alzheimer's, Parkinson's, Huntington's and motor neuron diseases (3,4). Tools that can measure proteostasis imbalance therefore offer capacity to explore the mechanisms involved.

Previously we developed a method that enabled a measure of the effectiveness of the quality control system in maintaining protein homeostasis (5). The method involved the use of a biosensor that comprised of a model protein that engages with protein quality control machinery such as chaperones. The biosensor reported on amount of the model protein bound to quality control proteins (which we call hereon call holdase activity) and on the ability of quality control proteins to repress inappropriate protein aggregation of the model protein. The model protein was a catalytically inactive variant of the prokaryotic RNAse barnase. Unfolded barnase is both permissive to aggregation and able to bind to Hsp70 and Hsp40 family chaperones (6). Barnase folding resembles a 2-state mechanism and the proportion of unfolded barnase relative to folded barnase can be predictably tuned by mutation (7). Hence a panel of barnase variants enable different biosensors tuned to different ratios of folded versus unfolded proteins. When the biosensor is expressed in cells the proportion of folded proteins can be measured by fluorescence resonance energy transfer (FRET) through N- and C- terminal fusions to fluorescent protein donors and acceptors (**Fig 1A**). We previously showed that the abundances of unfolded barnase is increased in cells relative to that predicted by analysis of purified proteins due to quality control machinery forming complexes with the unfolded-like conformations of the biosensor and partitioning it from the equilibrium of folding (6). Therefore, alterations in quality control levels influence the total abundance of unfolded-like barnase, which we can detect by FRET, and therefore determine changes in the overall quality control supply available as a measure of proteostasis capacity.

The amount of biosensor aggregation can also provide a measure of overall chaperone activity. Our prior work devised a strategy that quantitatively measured aggregation as a complementary approach to foldedness (6). Here, we applied our biosensor system to examine how proteostasis balance is affected specifically within the nucleus and cytosol. We examine these local proteostasis changes that result from different triggers of stress either globally to the cell or locally within the cytoplasm or nucleus.

65

Results

Generation of nuclear targeted biosensors and validation of folding stabilities

The biosensor system comprises a suite of constructs whereby the barnase moiety has been mutated to display different standard free energies of folding ($\Delta G^0{}_F$), which define the thermodynamic equilibrium of folding K_f (**Fig 1B**). These constructs contained a nuclear export sequence (NES), which leads to them being restricted to a cytosolic localization (6). To direct the constructs to the nucleus we removed the NES and fused a nuclear localization sequence (NLS) from the SV40 protein to the N-terminus (**Fig 1A; Table 1** for sequences used). The biosensor containing wild-type* (WT*) barnase (which is marked with * to denote it contains the catalytic inactivation mutation H102A that is used in all our constructs) was efficiently targeted into the nucleus (**Fig 1C**). All mutants of barnase showed a similar result (not shown).

Because the NLS and NES could themselves affect the folding equilibrium, we measured their effect on folding by a urea denaturation curve which showed no noticeable difference (**Fig 1D**). Hence, we concluded that the biosensors with NLS and NES are amenable to directly measure and compare protein homeostasis balances between the cytosol and nucleus.

The strategy to monitor both the abundances of unfolded barnase and aggregation behaviour involved a flow cytometry protocol we previously developed (6). In essence, cells expressing the biosensor bifurcate into two distinct FRET populations when cells are gated on acceptor fluorescence versus donor fluorescence. The donor fluorescence levels are proportional to expression level and FRET and both are approximately linearly dependent on the acceptor fluorescence. One of the populations comprises a "lower slope" FRET population that contains cells with only soluble barnase biosensor (i.e. a mixture of medium and low FRET states; **Fig 1A and E**), whereas the other contains an "upper slope" FRET population, which contains cells with aggregated biosensor (i.e. dominated by high FRET states) (6). The gradient of the lower slope population is proportional to the actual FRET value and hence informative to the abundance of unfolded barnase versus folded barnase (i.e. the average signal of low and medium FRET states from **Fig 1A**). We had previously shown that quality control machinery such as Hsp70 and Hsp40 proteins HSPA8 and DNAJB1, respectively, can bind to unfolded biosensor and hold it in an unfolded-like state that has a low FRET signal (6) as summarized conceptually in **Fig 1A**. This binding creates a pool of chaperone-bound biosensor that is partitioned from the equilibrium of folding. Greater partitioning leads to lower FRET signals, which can thus be used as a measure of the capacity of the quality control system to engage with the biosensor.

98 First, we examined whether the cytosolic and nuclear environments differentially affected the FRET

99 readouts. This was achieved by expressing a FRET construct in which barnase was replaced with a

100 short linker sequence that was not expected to be affected by changes in conformation or other

101 ligand binding events. As such this linker should render the biosensor insensitive to folding-related

102 effects and hence measures off-target influences on FRET signal as previously described (6). The

103 linker control revealed a small (1.7%) but significant ($p < 0.0001$, Student's t-test; 2-tailed) decrease

104 in FRET in the nucleus compared to the cytosol between the NLS and NES tagged variants (**Fig 2A**).

105 To correct for this influence, all the subsequent analyses involving the barnase biosensors were

106 corrected for differences using the NLS and NES linker construct controls.

107 Next, we examined the effectiveness of protein quality control systems to interact with the

108 biosensor in the nucleus versus the cytosol. For this we examined four previously characterized

109 mutants of barnase in addition to wild-type* that have variable ΔG^0_F values and therefore different

110 proportions of folded to unfolded barnase at equilibrium (**Fig 1B**). After correction for off-target

111 FRET changes with the linker control, all nuclear-targeted biosensor variants had overall significantly

112 higher FRET values for the lower slope populations than the cytosol-targeted biosensors, except for

113 the most destabilised variant (I25A I96G), which is predicted to be substantially unfolded and

114 therefore possibly outside the dynamic range that can be detected (**Fig 2B**). The higher FRET values

115 in the nucleus are therefore indicative of less unfolded-like barnase conformations being held in

116 complex with chaperones that would otherwise be partitioned from the equilibrium of folding. The

117 results therefore suggested that the pool of chaperones that can bind to the biosensor is lower in

118 the nucleus than the cytosol.

119 To examine the aggregation propensity of the barnase biosensors, we applied our previously devised

120 method of determining the concentration of barnase at which 50% of the cells contain aggregates

121 ($A_{50\%}$) (6). $A_{50\%}$ values are derived from plots of the proportions of cells partitioning in the upper

122 slope for a given expression level of barnase in cells (**Fig 2C-D**). Consistent with prior findings (6),

123 WT* barnase did not aggregate and the less stable mutants (i.e. those with higher ΔG^0_F values) were

124 more sensitive to aggregation as determined by lower $A_{50\%}$ values (**Fig 2D**). For all the barnase

125 variants that aggregated, the $A_{50\%}$ values were lower in the nucleus compared to the cytosol (**Fig 2C-**

126 **D**). These results indicated that barnase is inherently more aggregation prone in the nucleus than

127 the cytosol, and therefore strengthens the conclusion that there are less quality control proteins in

128 the nucleus that are able to bind to and stabilize barnase and prevent aggregation.

129 **Hsp70 and Hsp40 chaperone systems more robustly mitigate unfolded proteins from aggregating**

130 **in the cytosol than the nucleus**

131   Hsp70 isoforms HSPA1B and HSPA8 were previously found in immunoprecipitation experiments as

132   major chaperone interactors to the destabilized barnase mutants (6). We found that related Hsp70

133   family member HSPA1A could modulate both the amount of unfolded-like barnase and the amount

134   of barnase aggregation, suggesting it could bind to and stabilize an unfolded-like conformation of

135   barnase (6). While these Hsp70 isoforms are highly abundant in the cytosol (8), it was unclear as to

136   how modulating their supply might propagate changes in the nucleus or cytosol.

137   To examine this question, we co-transfected HSPA1A and a specific Hsp40 cofactor DNAJB1 (9) with

138   the barnase biosensors and analysed the cells after 48 hours culture. The transfected HSPA1A and

139   DNAJB1 showed a mostly cytosolic enrichment (**Fig 3A**). The co-transfected chaperones significantly

140   reduced the biosensor lower slope gradients in the cytosol (**Fig 3B**), consistent with a greater

141   abundance of chaperone bound to unfolded barnase. The treatments also increased the $A_{50\%}$ values

142   indicating that the chaperones effectively suppressed inappropriate aggregation (**Fig 3C**). However,

143   these effects appeared more muted in the nucleus indicating that chaperone overexpression

144   preferentially deepens the pool of chaperone supply in the cytosol, which likely is explained by the

145   transfected chaperone being mostly restricted to the cytosol.

146   To further probe the role of Hsp70 activity we inhibited Hsp70 on cells (without overexpressed

147   chaperones) using the small molecule inhibitor VER-155008, which competitively binds to the ATP-

148   binding pocket of Hsp70 family proteins and impairs substrate binding (10). This treatment increased

149   the FRET values of the lower slope populations in the nucleus but not the cytosol (**Fig 3D**). This result

150   suggested that while Hsp40 and 70 proteins are more effective at binding barnase in the cytosol,

151   there was higher redundancy and flexibility in the cytosol to absorb a reduced Hsp70 activity than in

152   the nucleus. Hence the network appeared more vulnerable to collapse in the nucleus upon stresses

153   to proteostasis systems. However, the increased sensitivity to proteostasis imbalance in the nucleus

154   was not seen in terms of aggregation. Indeed, aggregation of the biosensor was far more

155   disproportionately enhanced in the cytosol than the nucleus (**Fig 3E**). These findings suggested that

156   the correlation of holdase activity and aggregation can be decoupled when specific elements of the

157   proteostasis network are impaired and that this effect may arise through redundant holdase activity

158   in the cytosol from non-Hsp70 chaperones that are overall less effective at preventing aggregation

159   than Hsp70.

160   **Aggregation of mutant Htt exon 1 in the cytosol propagates proteostasis imbalances in the cytosol**

161   **and nucleus**

162   Next we investigated the quality control supply in the nucleus and cytosol in the context of disease-

163   related protein misfolding and aggregation. For this we co-expressed the biosensors with mutant

164 Huntington exon 1 fragment containing 97 glutamines in the polyglutamine repeat sequence

165 (Httex1$_{97Q}$) fused to GFP, which forms cytosolic perinuclear inclusions in HEK293T cells (11). Mutant

166 Httex1 fragments with polyglutamine sequences longer than 36 glutamines accumulate into

167 inclusion bodies in neurons of Huntington Disease patients and have been implicated to direct a

168 maladaptation in protein quality control (12). Because the fluorescence of GFP interferes with our

169 capacity to monitor FRET, we used a variant of GFP that is non-fluorescent as characterized

170 previously (13) and also added a 6 amino acid tetracysteine motif for post hoc detection by ReAsH

171 biarsenical dye binding (14). Live cells were examined for inclusions, which were detectable as

172 spherical pearl-like structures under transmission imaging of confocal microscopy, imaged for FRET

173 and then post hoc analyzed by ReAsH staining to validate the inclusion structure. Because we

174 needed to fix the cells after imaging, which reduces ReAsH staining, we were not able to ascertain

175 cells containing only diffuse cytosolic Httex1$_{97Q}$. Using this approach, we observed the barnase

176 biosensor as enriched at the periphery of the inclusions suggesting a degree of co-aggregation or co-

177 recruitment to the inclusions (**Fig 4A**). This was both true for the WT* barnase biosensor, which does

178 not aggregate by its own volition, and for the nucleus-targeted biosensors suggesting that the

179 biosensors were kinetically trapped on the surface of the Httex1 inclusion. To assess whether the

180 biosensor was self-aggregated at the molecular scale we determined their FRET using a ratiometric

181 analysis of the fluorescence (**Fig 4A**). Indeed, the biosensor enriched at the inclusion periphery

182 appeared to have higher FRET than when more distal from the inclusions in either the nucleus or

183 cytosol. We further assessed the aggregation state using fluorescence recovery after photobleaching

184 (FRAP) (**Fig 4B**). A small section of the biosensor was targeted for bleaching on the periphery of the

185 Httex1 inclusion. Both nucleus and cytosol targeted biosensors showed little to no recovery after

186 bleaching, indicating the protein was in an immobile state on the seconds timescale (**Fig 4C**).

187 Because the aggregation of the biosensor at the periphery of the inclusion is a confounding factor in

188 whole cell fluorescence analysis by our flow cytometry methods, we instead measured FRET by

189 microscopy targeting small subregions of the cells away from the inclusions. This analysis revealed

190 that the presence of Httex1$_{97Q}$ inclusions had no bearing on the FRET of the WT* barnase biosensor

191 outside that associated with the inclusion periphery (**Fig 4D**). By contrast, the I88G barnase

192 biosensor showed significantly changed FRET values regions outside the Httex1$_{97Q}$ inclusions

193 compared to cells without inclusions at all. In the case of the I88G barnase biosensor targeted to the

194 cytosol, the FRET was increased, which suggested a reduced overall holdase activity of chaperones in

195 the cytosol arising from Httex1$_{97Q}$ aggregation. However, in the case of the I88G barnase biosensor

196 targeted to the nucleus the FRET was decreased. This result is consistent with an elevated holdase

197 activity in the nucleus when Httex1$_{97Q}$ aggregates form. This result therefore suggests when protein

198 aggregation occurs in the cytosol that cells can move the pool of quality control machinery from the

199 cytosol into the nucleus as part of a global coordinated stress response.

200

201 **Discussion**

202 Our studies show that the balance of resources required to manage proteostasis is different in the

203 cytosol relative to the nucleus. We find evidence for there being a lower supply of chaperone

204 capacity in the nucleus that is able to bind to the unfolded barnase and prevent its aggregation.

205 When we supplemented the cells with additional Hsp70 and Hsp40 protein by their overexpression

206 (HSPA1A and DNAJB1), we increased holdase activity in the cytosol and lowered the aggregation

207 potential consistent with these chaperones exerting a critical activity to bind unfolded proteins and

208 prevent their aggregation. When we pharmacologically inhibited the Hsp70 chaperone system we

209 observed a disproportionate impact on aggregation in the cytosol, concordant with the cytosol being

210 more richly dependent on Hsp40 and Hsp70 chaperone-based networks to prevent protein

211 aggregation.

212 Overall, these results are consistent with the greater requirement of the Hsp70 chaperone system to

213 engage with unfolded or aggregation-prone proteins in the cytosol. This finding is consistent with

214 the high abundance of these chaperones in the cytosol (8), which is not surprising given that most

215 proteins are synthesized in the cytosol or endoplasmic reticulum.

216 Our findings with mutant Httex1$_{97Q}$ indicate that the aggregation in the cytosol can manifest

217 dysfunction in quality control capacity in both the cytosol and nucleus. Consistent with prior findings

218 that protein aggregation can sequester quality control resources away from "housekeeping"

219 activities and lead to metastably-folded proteins aggregating (15), we found that the pool of

220 resources binding to unfolded barnase biosensor decreased in the cytosol. Prior studies have found

221 that Hsp70 and Hsp40 proteins are recruited into inclusions formed by Httex1$_{97Q}$ and similar proteins

222 with expanded polyglutamine sequences (16-19). One function for this recruitment may be

223 disaggregation, in light of recent findings showing the Hsp70 based chaperone machinery can

224 dissociate amyloid fibrils (20). More unexpected however was the finding that there was an increase

225 in unfolded barnase in the nucleus, which suggests that chaperones are redirected into the nucleus

226 under stress. Hsp70 is known to translocate from the cytosol into the nucleus upon heat shock (21-

227 23), suggesting there is a dynamic capacity for quality control machinery activity in the nucleus

228 under times of stress. This translocation is regulated by the Hikeshi nuclear import carrier, which is

229 crucial for cells to recover from heat shock stress (24). DNAJB1 can also deliver misfolded protein

230 into the nucleus for degradation (25).

231   The other notable result from our study was the recruitment of WT* barnase biosensor to the

232   Httex1$_{97Q}$ inclusion. We have never observed the wild-type* biosensor to aggregate when expressed

233   on its own suggesting that the inclusion provides a mechanism to recruit this protein to the surface.

234   One interesting possibility is that a small fraction of the biosensor remains in complex with

235   chaperones; and that these complexes are recruited to the surface of the inclusion by Hsp70 -based

236   triage mechanisms that more generally handle misfolded proteins in the cell. The different extent of

237   WT* biosensor foldedness in the nucleus compared to the cytoplasm supports the conclusion that

238   some of the wild-type barnase is partitioned from the equilibrium of folding in an unfolded-like

239   state. Discrete bodies containing misfolded protein including the JUNQ, aggresome and Q-bodies

240   have been proposed as cellular depots for processing protein aggregates, and are enriched with

241   different Hsp70 and Hsp40 proteins (26,27). In addition, Hsp70 has been proposed to engage with

242   the surface of protein aggregates to act as a disaggregase (20). Hence, the capture of wild-type*

243   biosensor may be indicative of a wider network of chaperone client interactions, protein aggregate

244   bodies in the cell and a broader interconnected quality control network. And thus chaperones may

245   have a broader function as a kind of lubricant constantly interfacing with unfolded proteins and

246   aggregating proteins.

247   **Materials and Methods**

248   **Expression constructs.** The cytosolic FRET barnase biosensor library expressed in the pTriEx4 vector

249   were prepared as previously described (5). In brief, the barnase moiety was flanked by circularly

250   permuted mTFP1 cp175 and Venus cp173 fluorescent proteins. Nuclear localised FRET barnase was

251   generated by the addition of a N-terminal SV40 NLS sequence to the original cytosolic barnase using

252   a synthesized gene cassette containing the relevant localization sequences (GeneArt (Thermofisher),

253   Waltham, Massachusetts) and standard restriction endonuclease-based ligation methods. For

254   generation of individual mutants of targeting biosensor, the WT* barnase biosensor kernel was

255   replaced by the barnase mutant of choice. This was achieved by double-digestion of both the

256   desired barnase mutant and nuclear targeting construct plasmids at BamHI and KpnI restriction

257   sites. The tetracysteine tagged Httex1 construct containing a tetracysteine tag at the C-terminus of

258   the Httex1 (TC1 (28)), and a non-fluorescent mutant of Emerald fluorescent protein (Em), Y66L (13),

259   was generated in-house to yield a plasmid named Httex1$_{97Q}$TC1-Em Y66L in the pT-Rex vector

260   (Invitrogen). The pT-Rex Em Y66L construct alone was also generated in-house as described

261   previously (13). V5-tagged chaperone proteins were overexpressed from pcDNA5/FRT/TO V5

262   DNAJB1 and pcDNA5/FRT/TO V5 HSPA1A provided as gifts from Harm Kampinga (29).via Addgene,

263   Watertown, Massachusetts.

264   **Cell culture.** HEK293T cells were maintained in DMEM supplemented with 10% (w/v) fetal calf

265   serum and 1 mM glutamine in a 37°C humidified incubator with 5% v/v atmospheric CO_2. Cells were

266   seeded in poly-L-lysine coated plates. For microscopy experiments cells were plated at 3×10^5

267   cells/ml in an 8 well μ-slide (Ibidi, Martinsreid, Germany). For flow cytometry experiments cells were

268   seeded at 1.1×10^5 cells/ml in a 48 well plate. Cells were transiently transfected with Lipofectamine

269   3000 reagent as per manufacturer's instructions (Life Technologies, Thermofisher). For Barnase and

270   Httex1 co-transfections, the transfection was done in a way to decouple the expression of the two

271   plasmids.

272   HSP70 was inhibited with 20 μM VER-155008 (cat #SML0271, Sigma-Aldrich, St. Louis, Missouri) in

273   culture media for 18 h.

274   **Microscopy.** Cells were imaged on a TCS SP5 confocal microscope (Leica Biosystems, Nussloch,

275   Germany). For immunofluorescence, cells were fixed in 4% w/v paraformaldehyde for 15 mins at

276   room temperature, washed with phosphate buffered saline (PBS), and permeabilized in 0.5% v/v

277   Triton X-100 in PBS (Sigma-Aldrich) for 30 mins. After incubation in blocking solution (5% w/v bovine

278   serum albumin in 0.3% v/v Triton X-100 in PBS), cells were incubated with anti-V5 (1:250 dilution in

279   1% w/v bovine serum albumin in 0.3% v/v Triton X-100 in PBS) (cat #ab27671, Abcam, Cambridge,

280   United Kingdom) overnight at 4°C. Cells were then washed in 1% w/v ovine serum albumin in 0.3%

281   v/v Triton X-100 in PBS before being stained with anti-mouse cy5 (1:500 dilution in PBS) for 30 min

282   at room temperature. Prior to confocal imaging, cells were stained with Hoechst 33342

283   (ThermoFisher).

284   **Image analysis.** Confocal images were analysed using custom analysis scripts for FIJI (30) and

285   Python (v 3.6.7), available alongside example datasets at doi.org/10.5281/zenodo.4686851.

286   In the case of immunofluorescence measurements, whole cells and nuclei were initially identified

287   using the machine learning package CellPose (31) . Segmentation was performed on the Cy5-labelled

288   anti-V5 antibody and Hoechst channels (633 nm excitation, 650-750 nm emission and 405 nm

289   excitation, 410-450 nm emission respectively) to identify the whole cell and nuclei regions of

290   interest (ROI) respectively. Per-pixel information for each ROI was then collected and the nuclei ROIs

291   removed from the whole cell to yield the cytosolic population. Finally, the fluorescence intensity for

292   the nucleus and cytosol was determined from the mean of all pixels in each compartment.

293   To quantify fluorescence recovery after photobleaching (FRAP), ROI for individual bleach spots were

294   defined via automatic Otsu thresholding of the first bleaching frame. Identical ROI's were then

295   manually placed for the adjacent (non-bleached) and background regions. Where necessary, ROI

296   positions were manually adjusted across timepoints to account for cellular drift. The mean intensity

297   was calculated for each ROI, and both bleached and non-bleached ROIs were then corrected against

298   the corresponding background ROI for each time point, generating B_{corr} and NB_{corr} respectively. The

299   ratio of B_{corr} / NB_{corr} at each time point was finally normalised to the pre-bleach ratio of B_{corr} / NB_{corr}

300   to yield the relative recovery.

301   In the case of FRET measurements, whole cells, nuclei and Httex1 inclusions were initially identified

302   using CellPose (31) as described above. In this case, segmentation was performed on the acceptor

303   channel (488 nm excitation, 510–560 nm emission), computationally inverted acceptor channel and

304   ReAsH channel (561 nm excitation, 610–680 nm emission) for whole cells, nuclei and inclusions

305   respectively. After manual inspection to ensure the accuracy of each round of segmentation, per-

306   pixel intensity values for each ROI were collected. In the case of cytosolic barnase variants, both the

307   nuclei and aggregate features were excluded from the whole cell to yield the diffuse barnase

308   population. In the case of nuclear barnase variants, any aggregate ROI within the nuclei ROI were

309   similarly excluded to yield the diffuse barnase population. Finally, the relative FRET for each ROI was

310   calculated as the mean per-pixel intensity in the FRET channel (458 nm excitation, 510-560 nm

311   emission).

312   **Flow cytometry.** After 24 h (drug treatments) or 48 h (co-transfections) post-transfection, cells were

313   washed and harvested by gentle pipetting in PBS. Cells were analysed via flow cytometry as

314   described previously (6). In short, 150 µl of cell suspension was analysed at flowrate of 3 µl/sec on a

315   BD LSRFortessa cell analyser (BD Biosciences, North Ryde, NSW, Australia). Acceptor (Venus)

316   fluorescence was collected with the 488 nm laser and FITC (530/30) filter. Acceptor sensitized

317   emission (FRET) and donor (mTFP1) fluorescence were collected with the 405 nm laser with PE

318   (575/25) and V500 (525/50) filters, respectively. All flow cytometry data were processed with FlowJo

319   (version 10, Tree Star Inc, Ashland, Oregon) to exclude cell debris, cell aggregates and untransfected

320   cells. The Venus channel was compensated to remove bleed through from mTFP1 and FRET channels

321   using donor only. Data were analysed in MATLAB (version 9, MathWorks, Natick, Massachusetts).

322   The gating strategy and associated data analysis protocols are detailed previously (32).

323   **Urea denaturation curves.** Urea denaturation curves were measured on cell lysates expressing the

324   biosensors in 96 well format. In essence, 80 µl of samples were prepared containing 0 M to 8 M urea

325   in PBS. Lysates were prepared from cells 24 h after transfection (wild-type* with NES and NLS tags)

326   by pipetting in 20 mM Tris pH 8.0, 2 mM MgCl$_2$, 1% v/v Triton X-100, 1 × EDTA-free protease inhibitor

327   (Roche, Basel, Switzerland), 150 mM NaCl, 20 U ml^{-1} benzonase, 1 mM PMSF. Aggregates and cell

328   debris were pelleted by centrifugation at 16,000 g for 10 min at 4 °C. 5 µl supernatant was added to

329   each urea concentration. As the measurements were ratiometric and both fluorophores were on the

330   same molecule, samples were not matched for protein concentration. Fluorescence readings

331   (430 nm excitation, 492 nm emission and 532 nm emission) were measured at 23 °C using a

332   Clariostar microplate reader (BMG Labtech, Mornington, Victoria, Australia) every 15 min for 4 h.

333   Relative FRET efficiencies (calculated as Acceptor fluorescence/[Donor fluorescence + Acceptor

334   fluorescence]) were averaged across readings and fit to a two-state unfolding model as described

335   previously (6).

336

337   **References**

338   1.   Schneider, K., and Bertolotti, A. (2015) Surviving protein quality control catastrophes--from
339   cells to organisms. *J. Cell Sci.* **128**, 3861-3869
340   2.   Knowles, T. P., Vendruscolo, M., and Dobson, C. M. (2014) The amyloid state and its
341   association with protein misfolding diseases. *Nat Rev Mol Cell Biol* **15**, 384-396
342   3.   Bertram, L., and Tanzi, R. E. (2005) The genetic epidemiology of neurodegenerative disease.
343   *J. Clin. Invest.* **115**, 1449-1457
344   4.   Hipp, M. S., Park, S. H., and Hartl, F. U. (2014) Proteostasis impairment in protein-misfolding
345   and -aggregation diseases. *Trends Cell Biol.* **24**, 506-514
346   5.   Wood, R. J., Ormsby, A. R., Radwan, M., Cox, D., Sharma, A., Vöpel, T., Ebbinghaus, S.,
347   Oliveberg, M., Reid, G. E., Dickson, A., and Hatters, D. M. (2018) A biosensor-based
348   framework to measure latent proteostasis capacity. *Nature Communications* **9**, 287
349   6.   Wood, R. J., Ormsby, A. R., Radwan, M., Cox, D., Sharma, A., Vopel, T., Ebbinghaus, S.,
350   Oliveberg, M., Reid, G. E., Dickson, A., and Hatters, D. M. (2018) A biosensor-based
351   framework to measure latent proteostasis capacity. *Nat Commun* **9**, 287
352   7.   Serrano, L., Kellis, J. T., Jr., Cann, P., Matouschek, A., and Fersht, A. R. (1992) The folding of
353   an enzyme. II. Substructure of barnase and the contribution of different interactions to
354   protein stability. *J. Mol. Biol.* **224**, 783-804
355   8.   Finka, A., and Goloubinoff, P. (2013) Proteomic data from human cell cultures refine
356   mechanisms of chaperone-mediated protein homeostasis. *Cell Stress Chaperones* **18**, 591-
357   605
358   9.   Kampinga, H. H., and Craig, E. A. (2010) The HSP70 chaperone machinery: J proteins as
359   drivers of functional specificity. *Nature Reviews Molecular Cell Biology* **11**, 579-592
360   10.   Schlecht, R., Scholz, S. R., Dahmen, H., Wegener, A., Sirrenberg, C., Musil, D., Bomke, J.,
361   Eggenweiler, H. M., Mayer, M. P., and Bukau, B. (2013) Functional analysis of Hsp70
362   inhibitors. *PLoS One* **8**, e78443
363   11.   Ramdzan, Y. M., Trubetskov, M. M., Ormsby, A. R., Newcombe, E. A., Sui, X., Tobin, M. J.,
364   Bongiovanni, M. N., Gras, S. L., Dewson, G., Miller, J. M. L., Finkbeiner, S., Moily, N. S., Niclis,
365   J., Parish, C. L., Purcell, A. W., Baker, M. J., Wilce, J. A., Waris, S., Stojanovski, D., Bocking, T.,
366   Ang, C. S., Ascher, D. B., Reid, G. E., and Hatters, D. M. (2017) Huntingtin Inclusions Trigger
367   Cellular Quiescence, Deactivate Apoptosis, and Lead to Delayed Necrosis. *Cell Rep* **19**, 919-
368   927
369   12.   Cox, D., Raeburn, C., Sui, X., and Hatters, D. M. (2020) Protein aggregation in cell biology: An
370   aggregomics perspective of health and disease. *Semin. Cell Dev. Biol.* **99**, 40-54
371   13.   Olshina, M. A., Angley, L. M., Ramdzan, Y. M., Tang, J., Bailey, M. F., Hill, A. F., and Hatters, D.
372   M. (2010) Tracking mutant huntingtin aggregation kinetics in cells reveals three major
373   populations that include an invariant oligomer pool. *J. Biol. Chem.* **285**, 21807-21816
374   14.   Ramdzan, Y. M., Polling, S., Chia, C. P., Ng, I. H., Ormsby, A. R., Croft, N. P., Purcell, A. W.,
375   Bogoyevitch, M. A., Ng, D. C., Gleeson, P. A., and Hatters, D. M. (2012) Tracking protein
376   aggregation and mislocalization in cells with flow cytometry. *Nat Methods* **9**, 467-470
377   15.   Gidalevitz, T., Ben-Zvi, A., Ho, K. H., Brignull, H. R., and Morimoto, R. I. (2006) Progressive
378   disruption of cellular protein folding in models of polyglutamine diseases. *Science* **311**, 1471-
379   1474
380   16.   Mitsui, K., Nakayama, H., Akagi, T., Nekooki, M., Ohtawa, K., Takio, K., Hashikawa, T., and
381   Nukina, N. (2002) Purification of polyglutamine aggregates and identification of elongation
382   factor-1alpha and heat shock protein 84 as aggregate-interacting proteins. *J. Neurosci.* **22**,
383   9267-9277
384   17.   Hay, D. G., Sathasivam, K., Tobaben, S., Stahl, B., Marber, M., Mestril, R., Mahal, A., Smith, D.
385   L., Woodman, B., and Bates, G. P. (2004) Progressive decrease in chaperone protein levels in
386   a mouse model of Huntington's disease and induction of stress proteins as a therapeutic
387   approach. *Hum. Mol. Genet.* **13**, 1389-1405

388 18. Seidel, K., Meister, M., Dugbartey, G. J., Zijlstra, M. P., Vinet, J., Brunt, E. R., van Leeuwen, F.
389   W., Rub, U., Kampinga, H. H., and den Dunnen, W. F. (2012) Cellular protein quality control
390   and the evolution of aggregates in spinocerebellar ataxia type 3 (SCA3). *Neuropathol. Appl.*
391   *Neurobiol.* **38**, 548-558
392 19. Radwan, M., Lilley, J. D., Ang, C. S., Reid, G. E., and Hatters, D. M. (2020) Immiscible inclusion
393   bodies formed by polyglutamine and poly(glycine-alanine) are enriched with distinct
394   proteomes but converge in proteins that are risk factors for disease and involved in protein
395   degradation. *PLoS One* **15**, e0233247
396 20. Nillegoda, N. B., Kirstein, J., Szlachcic, A., Berynskyy, M., Stank, A., Stengel, F., Arnsburg, K.,
397   Gao, X., Scior, A., Aebersold, R., Guilbride, D. L., Wade, R. C., Morimoto, R. I., Mayer, M. P.,
398   and Bukau, B. (2015) Crucial HSP70 co-chaperone complex unlocks metazoan protein
399   disaggregation. *Nature* **524**, 247-251
400 21. Pelham, H. R. (1984) Hsp70 accelerates the recovery of nucleolar morphology after heat
401   shock. *EMBO J.* **3**, 3095-3100
402 22. Welch, W. J., and Feramisco, J. R. (1984) Nuclear and nucleolar localization of the 72,000-
403   dalton heat shock protein in heat-shocked mammalian cells. *Journal of Biological Chemistry*
404   **259**, 4501-4513
405 23. Velazquez, J. M., and Lindquist, S. (1984) hsp70: nuclear concentration during environmental
406   stress and cytoplasmic storage during recovery. *Cell* **36**, 655-662
407 24. Kose, S., Furuta, M., and Imamoto, N. (2012) Hikeshi, a nuclear import carrier for Hsp70s,
408   protects cells from heat shock-induced nuclear damage. *Cell* **149**, 578-589
409 25. Park, S. H., Kukushkin, Y., Gupta, R., Chen, T., Konagai, A., Hipp, M. S., Hayer-Hartl, M., and
410   Hartl, F. U. (2013) PolyQ proteins interfere with nuclear degradation of cytosolic proteins by
411   sequestering the Sis1p chaperone. *Cell* **154**, 134-145
412 26. Kaganovich, D., Kopito, R., and Frydman, J. (2008) Misfolded proteins partition between two
413   distinct quality control compartments. *Nature* **454**, 1088-1095
414 27. Sontag, E. M., Vonk, W. I. M., and Frydman, J. (2014) Sorting out the trash: the spatial nature
415   of eukaryotic protein quality control. *Curr. Opin. Cell Biol.* **26**, 139-146
416 28. Ramdzan, Y. M., Nisbet, R. M., Miller, J., Finkbeiner, S., Hill, A. F., and Hatters, D. M. (2010)
417   Conformation sensors that distinguish monomeric proteins from oligomers in live cells.
418   *Chem. Biol.* **17**, 371-379
419 29. Hageman, J., and Kampinga, H. H. (2009) Computational analysis of the human
420   HSPH/HSPA/DNAJ family and cloning of a human HSPH/HSPA/DNAJ expression library. *Cell*
421   *Stress Chaperones* **14**, 1-21
422 30. Rueden, C. T., Schindelin, J., Hiner, M. C., DeZonia, B. E., Walter, A. E., Arena, E. T., and
423   Eliceiri, K. W. (2017) ImageJ2: ImageJ for the next generation of scientific image data. *BMC*
424   *Bioinformatics* **18**, 529
425 31. Stringer, C., Wang, T., Michaelos, M., and Pachitariu, M. (2021) Cellpose: a generalist
426   algorithm for cellular segmentation. *Nat Methods* **18**, 100-106
427 32. Hatters Danny, Wood Rebecca, Raeburn Candice, Ormsby Angelique, Mikael Oliveberg, and
428   Alex, D. (2018) Measuring proteostasis capacity using transiently transfected bait proteins by
429   flow cytometry. *28 March 2018, Protocol Exchange(Version 1) available at Protocol*
430   *Exchange*

431

432

433

434

435 **Table 1. Sequence overview of the barnase biosensor constructs***

pTriEx4 barnase WT* + NES

MAHHHHHHGSGEQKLISEEDLGSGSGS**GGHHRVDFKTIYRAKKAVKLPDYHFVDHRIEILNHDKDYNKVTVYE SAVARNSTDGMDELYKGASGGMVSKGEETTMGVIKPDMKIKLKMEGNVNGHAFVIEGEGEGKPYDGTNTIN LEVKEGAPLPFSYDILTTAFAYGNRAFTKYPDDIPNYFKQSFPEGYSWERTMTFEDKGIVKVKSDISMEEDSFIYE IHLKGENFPPNGPVMQKKTTGWDASTERMYVRDGVLKGDVKHKLLLEG**SGAQVINTFDGVADYLQTYHKLPD NYITKSEAQALGWVASKGNLADVAPGKSIGGDIFSNREGKLPGKSGRTWREADINYTSGFRNSDRILYSSDWLIYK TTDAYQTFTKIRAAA*MDGGVQLADHYQQNTPIGDGPVLLPDNHYLSYQSALSKDPNEKRDHMVLLEFVTAAGIT LGMDELYKGGSGGMVSKGEELFTGVVPILVELDGDVNGHKFSVSGEGEGDATYGKLTLKLICTTGKLPVPWPTLV TTLGYGLMCFARYPDHMKQHDFFKSAMPEGYVQERTIFFKDDGNYKTRAEVKFEGDTLVNRIELKGIDFKEDGNI LGHKLEYNYNSHNVYITADKQKNGIKANFK*IRHNIEGTDILQKKLEELELDE

pTriEx4 barnase WT* + NLS

MCGGGPKKKRKVEDPGGSGS**GGHHRVDFKTIYRAKKAVKLPDYHFVDHRIEILNHDKDYNKVTVYESAVARN STDGMDELYKGASGGMVSKGEETTMGVIKPDMKIKLKMEGNVNGHAFVIEGEGEGKPYDGTNTINLEVKEG APLPFSYDILTTAFAYGNRAFTKYPDDIPNYFKQSFPEGYSWERTMTFEDKGIVKVKSDISMEEDSFIYEIHLKGE NFPPNGPVMQKKTTGWDASTERMYVRDGVLKGDVKHKLLLEG**SGAQVINTFDGVADYLQTYHKLPDNYITKS EAQALGWVASKGNLADVAPGKSIGGDIFSNREGKLPGKSGRTWREADINYTSGFRNSDRILYSSDWLIYKTTDAY QTFTKIRAAA*MDGGVQLADHYQQNTPIGDGPVLLPDNHYLSYQSALSKDPNEKRDHMVLLEFVTAAGITLGMD ELYKGGSGGMVSKGEELFTGVVPILVELDGDVNGHKFSVSGEGEGDATYGKLTLKLICTTGKLPVPWPTLVTTLGY GLMCFARYPDHMKQHDFFKSAMPEGYVQERTIFFKDDGNYKTRAEVKFEGDTLVNRIELKGIDFKEDGNILGHKL EYNYNSHNVYITADKQKNGIKANFK*IRHNIEGTKDEL

436 *Sequences coded as: **mTFP1 fluorescent protein (cp 175);** WT* barnase; *Venus fluorescent protein*

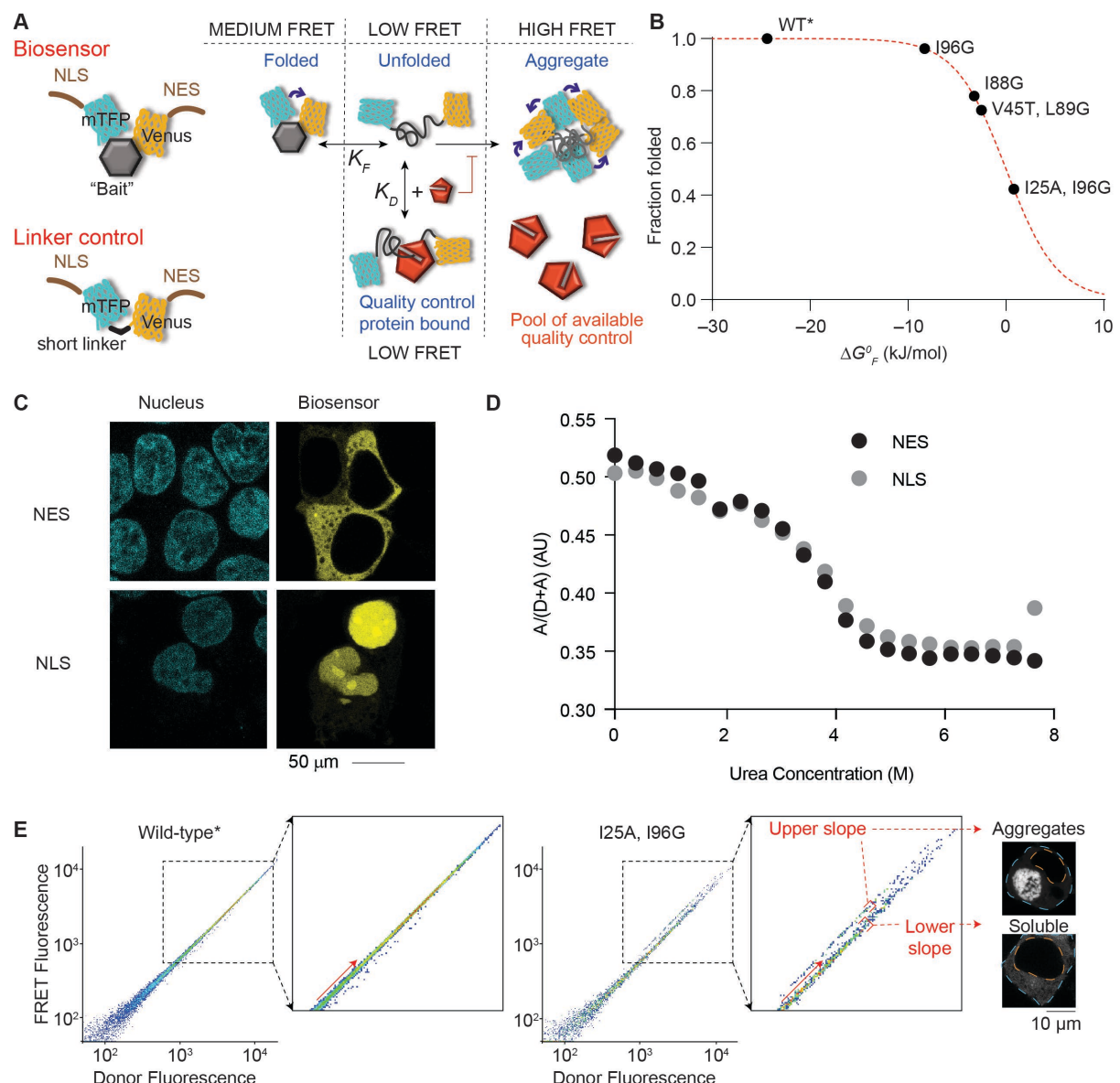437 *(cp 173);* NLS; NES

440

Figure 1: Targeting the barnase biosensor into the cytosol and nucleus. **A**. Schematic of how the biosensor works. The barnase protein is used as the "bait" for chaperones and is flanked with fluorescence proteins for Fluorescence Resonance Energy Transfer (FRET) measurements. A nuclear localization sequence (NLS) or nuclear export sequence (NES) is appended to the construct. The linker control has the barnase module omitted. **B**. Shown is the relationship between mutations in barnase, the effect on standard free energy of folding (ΔG^{o}_{F} at 20 °C), and predicted fraction folded for the various biosensor variants used in the study. Wild-type (WT) barnase is marked with * to denote it contains the catalytic inactivation mutation H102A. This mutation is present in all constructs in the study. **C.** Confocal images of HEK293T cells transiently transfected with either nuclear- or cytosol-targeting biosensor variant of the WT* barnase biosensor. The nucleus was visualized by Hoechst 33342 stain (cyan) and biosensor by Venus fluorescent protein fluorescence (yellow). **D.** Urea denaturation curves of WT* barnase biosensor variants as measured in cell lysates

453   by FRET. **E.** Flow cytometry strategy for monitoring foldedness and aggregation. Here the donor and

454   acceptor fluorescence of cells were measured by channels (FRET and Donor fluorescence was gated

455   by the PE (575/25) and V500 (525/50) filters, respectively with the 405 nm laser). The inset

456   highlights the changes that arise for cells bifurcated into "upper" and "lower" slope populations

457   (division shown with red arrow). Representative cells collected from gates corresponding to the

458   upper and lower slope populations imaged by confocal microscopy (grayscale). The orange dashed

459   line denotes the nucleus boundary and the cyan dashed line the cell boundary.

460

461

462
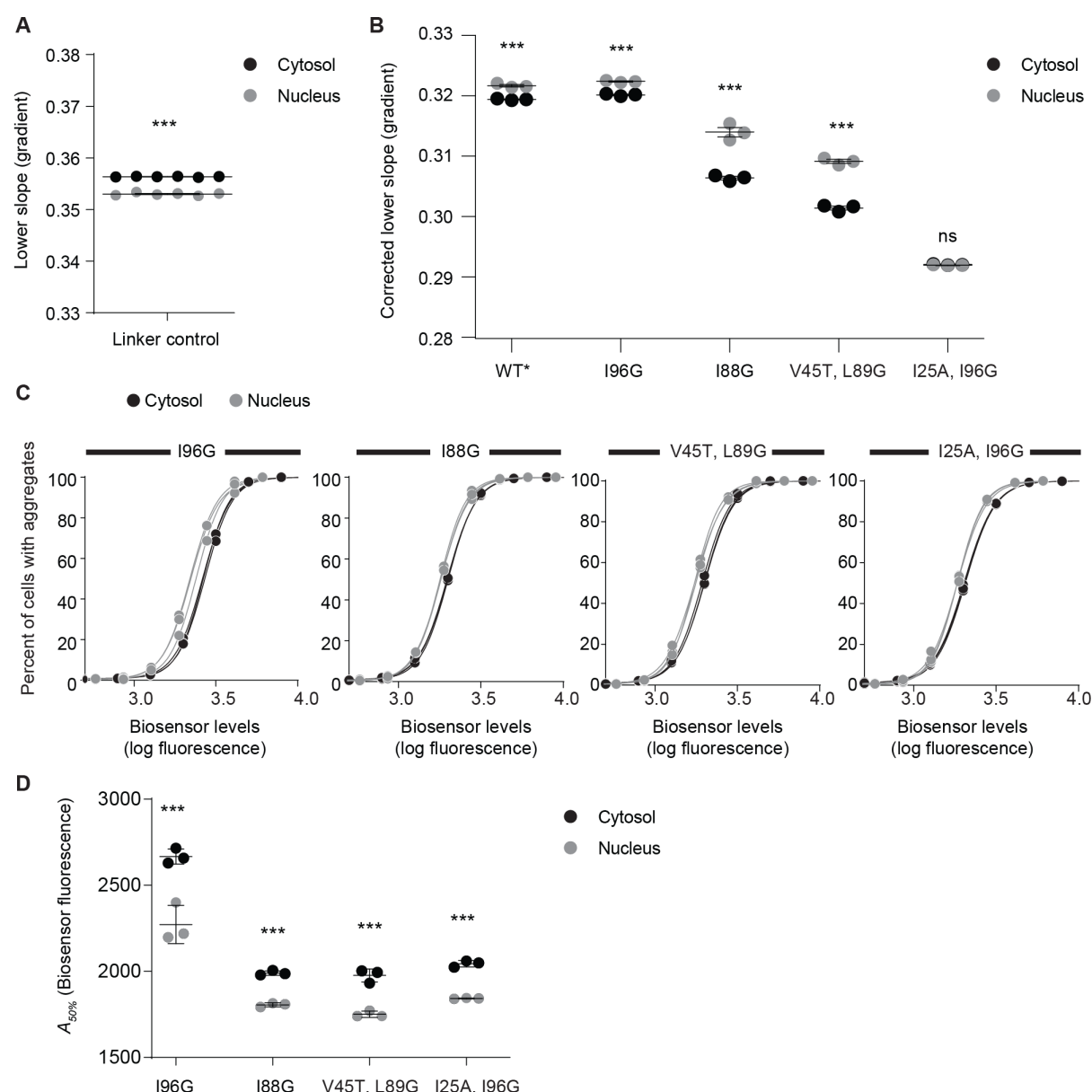
Figure 2: Reduced proteostasis resilience in the nucleus compared to the cytosol. All data in this figure relate to NLS or NES-tagged biosensor constructs transfected in HEK293 cells and analysed by flow cytometry. Individual biological replicates shown with means ± S.D. and with differences (nucleus v cytosol) assessed by Student's t-test (2-tailed); *** $p < 0.001$, ns => 0.05. **A.** Effect of intrinsic FRET differences in nucleus versus cytosol assessed with the linker control. **B.** Analysis of different barnase mutations. All data were corrected for background effects using the linker control. **C**. Assessment of aggregation. Shown are cells binned into different biosensor levels (based on Venus fluorescence) and each bin assessed for percent in upper slope versus lower slope populations. Curves are fits to Hill equation. Data were fitted independently within each replicate dataset (n=3). **D.** Shown are biosensor concentrations at which 50% of cells have aggregates ($A_{50\%}$), derived from the Hill equation fits shown in panel C.
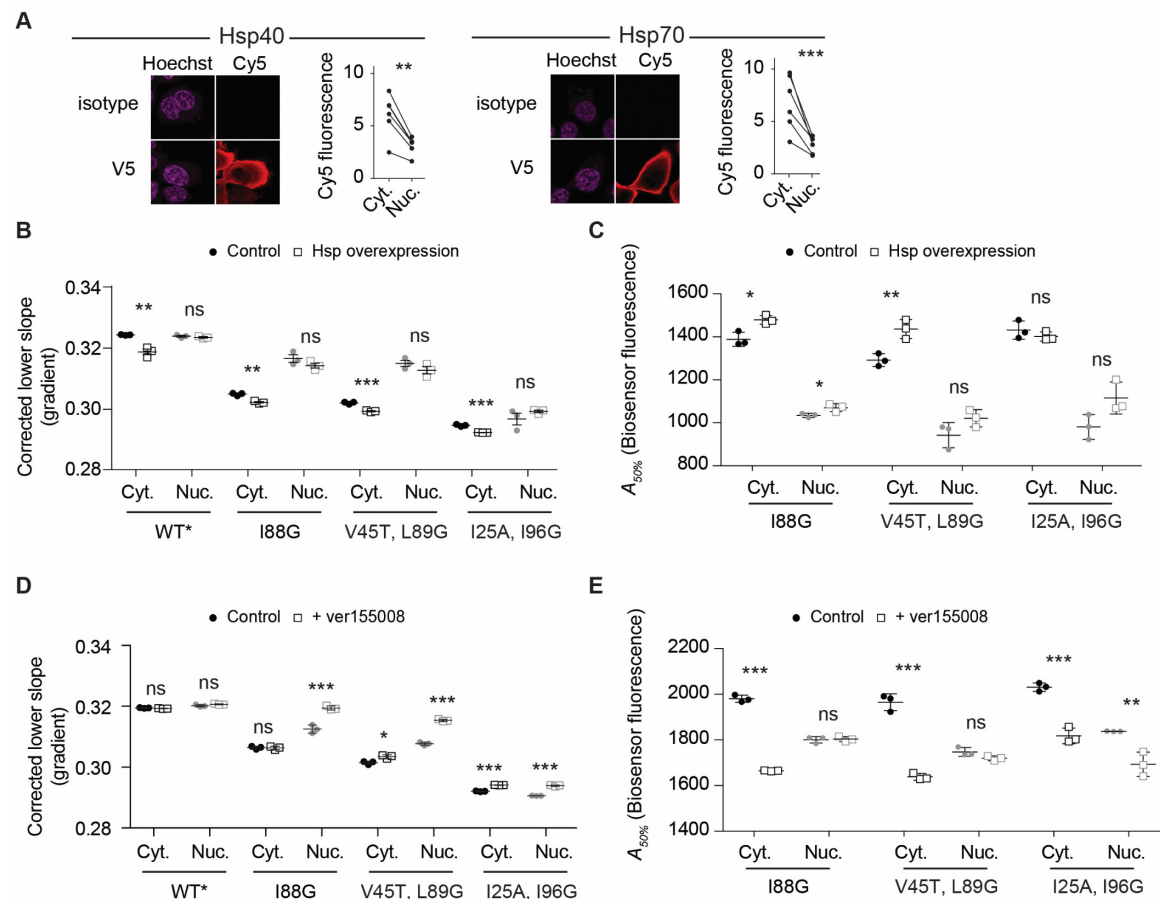
474

Figure 3: Cytosolic Hsp70 and Hsp40 activity provide depth in proteostasis resistance against protein misfolding and aggregation. A. Shown are immunofluorescence micrographs of HEK293T cells transiently transfected with either V5-tagged Hsp40 or Hsp70 proteins (DNAJB1 and HSPA1A respectively). The nucleus is stained with Hoechst 33342 and chaperone with Cy5 labelled anti-V5 antibody (or isotype control for specificity). Graphs indicate quantitation with paired Student's t-test results shown (2-tailed, paired); *** $p < 0.001$, ** $p < 0.01$. Data points represent immunofluorescence intensity in single cells (paired by mean cytosol and mean nucleus). **B.** Lower slope analysis by flow cytometry of HEK293 cells co transfected with the biosensors, DNAJB1 and HSPA1A or control (a non-fluorescent derivative of GFP (Y66L Emerald (13)) for 48 hours. Data points indicate biological replicates, bars indicate means ± S.D. Student's t-test results are shown (2-tailed; control v overexpression); *** $p < 0.001$, ** $p < 0.01$, * $p < 0.05$, ns => 0.05. **C.** Aggregation analysis ($A_{50\%}$) using the same treatments and conditions as for panel B. **D.** Lower slope analysis of HEK293 cells after transfection with the biosensors for 18 hours and a further treatment with 20 μM Hsp70 inhibitor VER-155008 for 18 h (versus vehicle control). Data is presented as per panel B. **E.** Aggregation analysis as presented for the other panels above.
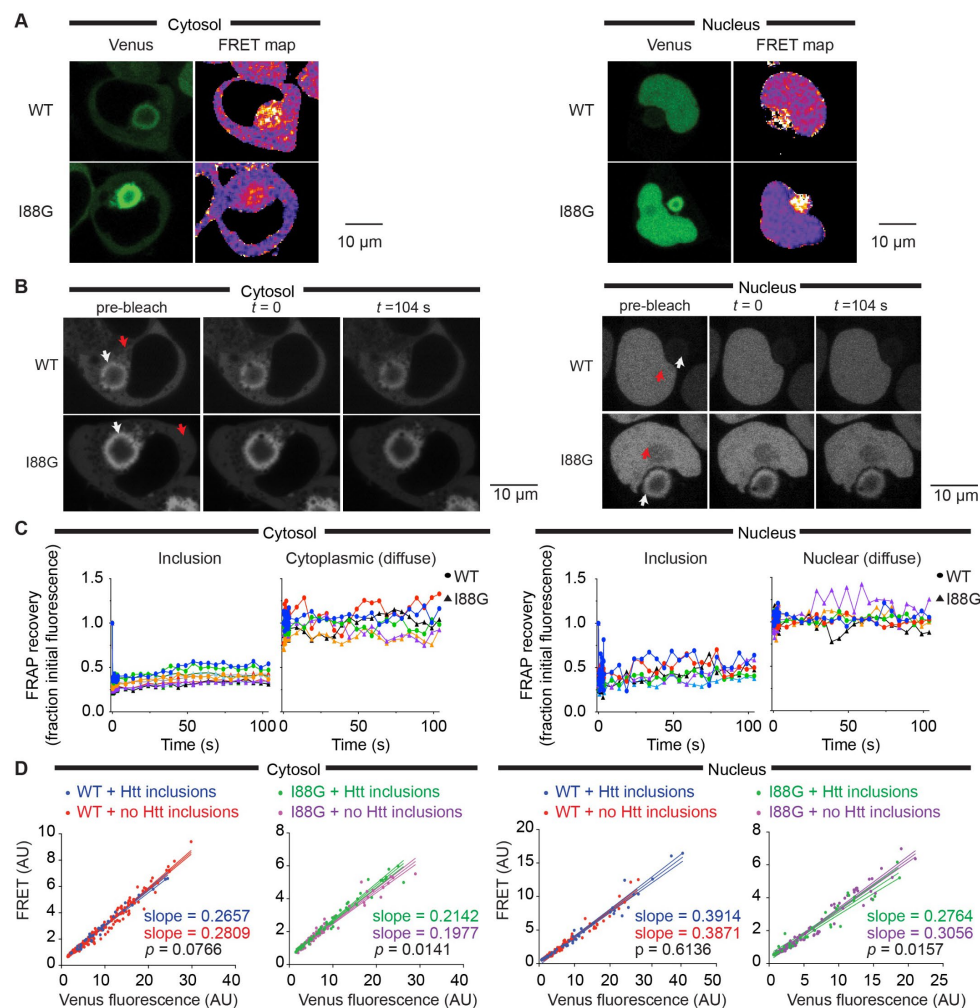
Figure 4: Huntingtin exon 1 aggregation in the cytosol manifests proteostasis imbalances in the nucleus and cytoplasm. A. Confocal micrographs showing the values proportional to the fluorescence ratio of acceptor/donor (Venus/mTFP) of the biosensors co-expressed with mutant Httex1$_{97Q}$ fused to a non-fluorescent mutant of GFP. Selected cells are those with Httex1 inclusions, identified post-hoc as described in the methods. Nuclear targeted biosensors are on the right and cytosolic targeted biosensors on the left (same format for each panel). The scale of the FRET map is colour coded from blue to magenta to yellow corresponding to lowest to highest FRET. **B.** Fluorescence recovery after photobleaching (FRAP) of biosensor at the periphery of the Httex1$_{97Q}$ inclusion. Arrows indicate region of bleaching. **C.** Quantitation of the data in panel B, tracking the recovery of fluorescence in the bleached zone. Each colour depicts the time course of an individual cell. **D.** Confocal microscopy FRET fluorescence values within cells distal to the inclusion. FRET fluorescence was measured by exciting at 458nm (mTFP1 excitation) and collecting the emission at 510-560 nm (Venus emission). Each dot represents the average fluorescence derived from a single cell value. Solid lines show line of best fit from a linear regression with dashed lines showing 95% confidence intervals. P-value was determined by two-tailed t-test.